Carpathian Journal of Earth and Environmental Sciences, August 2019, Vol. 14, No. 2, p. 311 - 322; DOI:10.26471/cjees/2019/014/082

THE GEOTHERMAL ENERGY OF THE EGYPTIAN RED SEA SHELF AS INFERRED FROM MAGNETIC DATA

Saada Ahmed SAADA & Sherif KHARBISH

Geology Department, Faculty of Science, Suez University, Suez, Egypt e-mail: saada.elsayed@suezuniv.edu.eg

Abstract: The Egyptian government tends to rely on renewable energy sources in the framework of sustainable development plans, including the geothermal energy. Therefore, this investigation objective to reveal the distribution of the geothermal energy in term of u-pwelling heat flow over the Egyptian Red Sea district from magnetic data by assessing the depth to the bottom of the magnetic bodies. The spectral analysis method was applied to the magnetic data to determine this bottom. This method demonstrates that the area is characterized by an average Curie depth of 9.5km. The calculated heat flow of this area (151 mW/m^2) goes above the common worldwide heat flow. The consequences establish a general increase of the Curie point depth from 7km, close to the axial trough, to 15km at the western coast. The assessed heat flow varies from 92 to about 196 mW/m^2. The examination area has a high geothermal gradient and a high heat flow because of the rifting action of the Red Sea that causes an up-welling heat flow from the upper mantle. The results indicate that the area is suitable for hydrocarbon accumulation as a source of non-renewable energy as well as geothermal energy as a source of renewable energy.

Key words*:* Red Sea; Curie point depth; geothermal gradient; heat flow; axial trough; spectral analysis.

1. INTRODUCTION

Egypt's geothermal zones are concentrated in the Gulf of Suez (GOS) region, where hot springs, such as Hammam Pharaum with a temperature of 71℃ and in the Red Sea (RS), where thermal wells such as Umm Khariga well with a temperature of 36°C (Said, 1962). The RS basin has an elongated shape lies among the uplifted Arabian-Nubian Shields. Moores et al., (1995) depicted it as a constricted oceanic basin that directly undergoes development amongst African and Arabian plates. The coastal shelves at both flanks of that sea slope in the direction of the main trough at depths exceed 1,000 m. The main trough includes the axial trough of approximately 30- 50km wide. The axial trough is characterized by disjointed deeps (Fig. 1) in the northern Red Sea (NRS), continuous in the central section while disappearing south of latitude14°N. Laughton (1970) exposed that the depths of that axial trough locally reach ~2,000 m. The research area (Fig. 1) comprises the northwestern offshore part of the Egyptian RS shelf.

The bathymetry of the RS exposes three different depth zones (Becker et al., 2009; Ligi et al., 2011; Schmidt et al., 2011; Smith & Sandwell, 1997), shallow shelves with a depth less than 50 m, deep shelves that ranges a depth from 500 to 1,000 m, and the main trough with depths range from 1,000 to about 3000m including the axial trough. Simply, fifteen percent of the RS forms the narrow main trough, which goes above 1,000 m in depth.

The heat flow (HF) studies that were done by Hosney (2001) and Morgan et al., (1980; 1983 and 1985) along the GOS- RS area gave also agreements of late volcanic action, which probably was the principal starting point of hydrothermal activity. They suggested the high HF of the GOS- RS rift up to 80-130 mW/m^2, which decreases laterally to attain a trademark estimation of ~46 mW/m^2 at ~90km away from the NRS axis because of the anomalous heated upper mantle (Feinstein et.al., 1996). Morgan & Swanberg (1979) recorded a general increase in the HF values in the northern part of Egypt in the direction of the RS coast, ranging from 36-55 mW/m^2 along the coast and 75-100 mW/m^2 at ~30-40km far from the shoreline. In addition, Girdler (1970) recorded an increase of the geothermal gradient (GG) of the RS toward the rift zone (Fig. 2). He confirmed an anomalously high gradient east to Quseir city. A similar value of ~80-100 mW/m^2 is consistent with the

observed low velocity below the Moho in the GOS (Gaulier et. al., 1988) and the average HF of the RS is 116 mW/m^2 (Boulos, 1990). Cochran et al., (1986) reasoned that the HF values change rapidly toward the rift-axis and an extreme value of 605 mW/m^2 as informed from the Conrad Deep region. Martinez & Cochran (1988) exhibited 191 HF measurements in the northerly RS along three crosses transversely the rift area. The HF across the rift steadily increases from values of ~125 mW/m^2 seaward of the coasts to usual values between 250 and 350 mW/m^2 was measured in the axial trough. This HF is greater than the world mean HF by 6-10 times (Makris & Rihm, 1991).

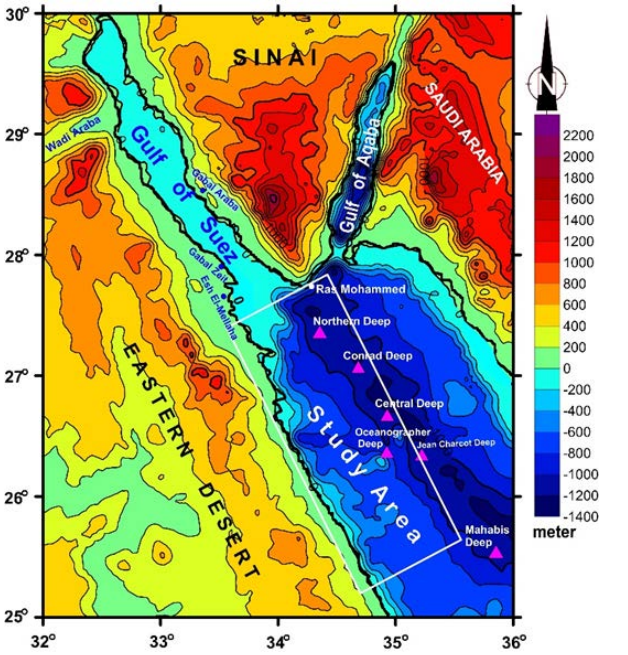

Figure 1. Topographic map of the NRS displays the research area and the primary deep brines (the dark blue color).

The HF around the River Nile in the northern portion of Egypt was examined, depending upon the density of different rocks and the velocity of the P-wave, by Hosney (2000). He detected a low HF (46 mW/m^2) at the west of the Nile area while the eastern part is a tectonically active province with a high HF up to 80-130 mWm^2 comprising the GOS and the northerly RS rifting regions. Saleh et al., (2013) estimated the Curie point depth (CPD) and the HF of the NRS. He linked them with the seismicity of that region. Their regional study includes 7˚latitudes×4˚ longitudes extending from the Nile valley to Saudi Arabia in the southern part and from Sinai to Jordan. They revealed that the CPD ranges from 5-20km and the maximum HF is about 235 mW/m^2 at Brothers Island and Conrad Deep due to their association with both the concentration of rifting to the axial trough and the magmatic activity at these parts. Salem et al. (2000) studied the HF of the area north Quseir City from magnetic data. They concluded a general increase of the HF exceeds 160 mW/m^2 to the east. Saada (2016a) calculated HF south to the present study area from the integration between 2D-modeling and spectral analysis of magnetic data. He showed that the HF values range from ~ 55 mW/m^2 at the exposed basement rocks in the western coastal area to more than 150 mW/m^2 close to the central trough. Elbarbary et al., (2018) estimated the HF of Egypt and revealed high values in the same direction.

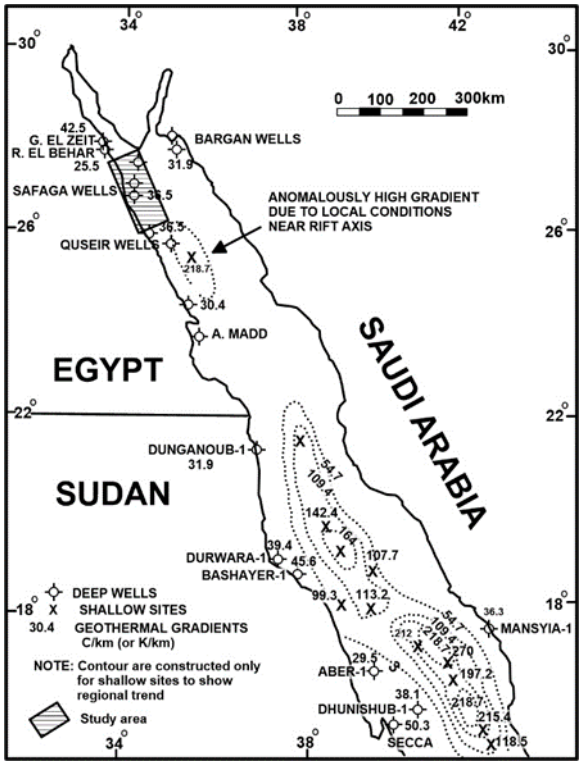

Figure 2. Geothermal Gradient Map of Red Sea (after Girdler, 1970).

The examination region includes the western half of the NRS, which is an active rifting zone. Consequently, this examination is completed to compute the GGs and the HF for this area. Some authors revealed that the NRS area involves a true seafloor spreading such as Vine (1966); Allan (1970); Roeser (1975); Egloff et al., (1991); Makris & Rihm (1991); Augustin et al., (2014); Mitchell & Park (2014);. Others confirmed that the region undergoes only stretching and thinning of the continental crust, without the formation of an actual oceanic crust (Cochran & Martinez 1988; Martinez & Cochran 1988; Cochran 2005). However, all of them have no doubt that this part is an active rifting area. It is significant to understand the HF along the western part that undergoes thinning of its continental crust due to that rifting.

Magnetic data are used for assessing the HF depends fundamentally on the calculation of the depth to the bottom of the magnetic sources that caused these anomalies. The depth of this bottom matches the Curie point isotherm at which the substance loses its magnetic polarization. Many scientists utilized the

examination of the magnetic data to appraise CPD in different areas. Among of them Smith et al., (1974); Bhattacharyya & Leu (1975); Byerly & Stolt (1977); Connard et al., (1983); Okubo et al., (1985); Blakely (1988); Tsokas et al., (1998); Tanaka et al., (1999). Recently, it was applied by many authors, e.g Maden et al., (2009); Trifonova et al., (2009); Kasidi & Nur (2012); Maden (2012); Saleh et al., (2013); Hsieh et al., (2014); Abraham et al., (2014 and 2015); Gao et al., (2015); Saada (2016a and 2016b). This procedure can be valuable as a quick examination technique for geothermal investigation goals, where magnetic data are presented in a great quantity.

This analysis goals to assess the CPD and the surface HF of the northern part of the Egyptian RS strip. To realize this goal, the filtering and spectral analysis techniques were applied to magnetic data of that area.

2. THE STUDY AREA

The formation of the RS can be divided into two main stages: a contractional tectonic stage that formed during 900 - 600 Ma, tailed with an extensional tectonic period during 595 - 575 Ma (Stern & Hedge, 1985; Miller & Dixon, 1992). A second compressional tectonic chapter resulted in crustal shortening of the Nubian Shield, which offset the east to northeast trending sutures in the northern portion of the shield (Abdelsalam & Stern, 1996) at Late Proterozoic. The greatest recent extensional tectonic episode of the African Nubian Shield is the formation of the RS, which took place in the Late Oligocene to Early Miocene since 30 Ma (Bosworth et al., 2005 and Ghebreab, 1998). The rift was connected with uplift that resulted in erosion of the sedimentary sequence and the underlying basement rocks (Avigad & Gvirtzman, 2009). The study area was affected by the Dead Sea-Gulf of Aqaba transform fault that is one of the greatest tectonically active features on the African Nubian Shield. It is a left-lateral strike-slip fault, which extends along about 1000km long. It has a slip rate varies between 1 and 10 mm/yr (Garfunkel, 1981 and Yeats *et al.,* 1997). Studying the Igneous activity and local subsidence along this transform fault, shows that this tectonic stage began in the Middle Miocene (ca. 18 Ma) with a whole displacement of nearly 105km (Garfunkel & Ben-Avraham, 1996).

The NRS cuts across a huge dome of Precambrian basement rocks (Arabian-Nubian massif) flanked by epicontinental and marine sedimentary rocks. The African and Arabian coastlines are nearly straight and parallel with a shore-to-shore width of approximately 180-190km (Allan, 1970; Martinez & Cochran, 1988). The morphology of the NRS has the general form of a broad basin with shallow marginal areas, stepping down toward a distinct zone of deeper water at ~1200-3000m referred to as the axial trough (Allan, 1970 and Cochran et al., 1986). The deeper axial trough is ~20-30km wide (Martinez & Cochran, 1989). The width of the main trough and the axial trough were reported by Cousteau et al., (1953) and Tazieff (1952).

The study area has certain small, isolated deeps (Fig. 1) inside the main trough (Ehrhardt & Hübscher, 2003). These deeps have water depth ranges from 1,000 and 1,400m where brines and sediments can accumulate (Hartmann, 1980 and Scholten et al., 1991). Some of these deeps contain hot or cold brines and metalliferous sediments (Backer & Schoell, 1972; Winckler et al., 2000) and localize coincident with or close to, high amplitude dipolar magnetic anomalies (Bertram et al., 2011; Botz et al., 2011). The well-known ones are the Shaban Deep, Conrad Deep, Klauke Deep, and Oceanographer Deep. Some of these axial “deeps” are the focus of the hydrothermal activity.

The lithology of study area includes two main groups, which are; the Precambrian basement and the Phanerozoic sedimentary rocks (Fig. 3). The Precambrian rocks contains gneisses and ophiolitic serpentinites, metagabbros, and metabasalts, as well as metasediments. These rocks were intruded by granitic rocks of older (gray) and younger (pink) granite, overlain by the Dokhan volcanics, and covered by molàsse-type sediments (Ries et al., 1983; Sultan et al., 1988; and Stern et al., 2004.

The sedimentary sequence of the NRS area is similar to that of the GOS. It was divided into three groups, which are pre-rift, syn-rift and post-rift sediments (Issawi et al., 1971; Montenat et al., 1988 and Said, 1990). The pre-rift subdivision includes intercalations of sandstone, shale, dolomite, and limestone ranging in age from Cambrian to Eocene. The syn-rift succession ranges from Late Oligocene to Pliocene for the onshore area but extends to Recent for the offshore part. This succession composes of Late Oligocene (Nakhil Formation), unconformably overlain by Early Miocene clastics of Ranga and carbonates of Um Mahara formations that corresponds to Thayiba, Nukhul, and Rudeis formations in the GOS subsurface, respectively. Middle and Late Miocene sediments with evaporites and clastics of Abu Dabbab and Marsa Alam formations overlie it conformable. These formations are corresponding to Kareem, Belayim, South Gharib, and Zeit of the GOS, respectively (Fig. 3). Because of the tectonic activity of the NRS, the constructed stratigraphic column displays at least five unconformities in the offshore area.

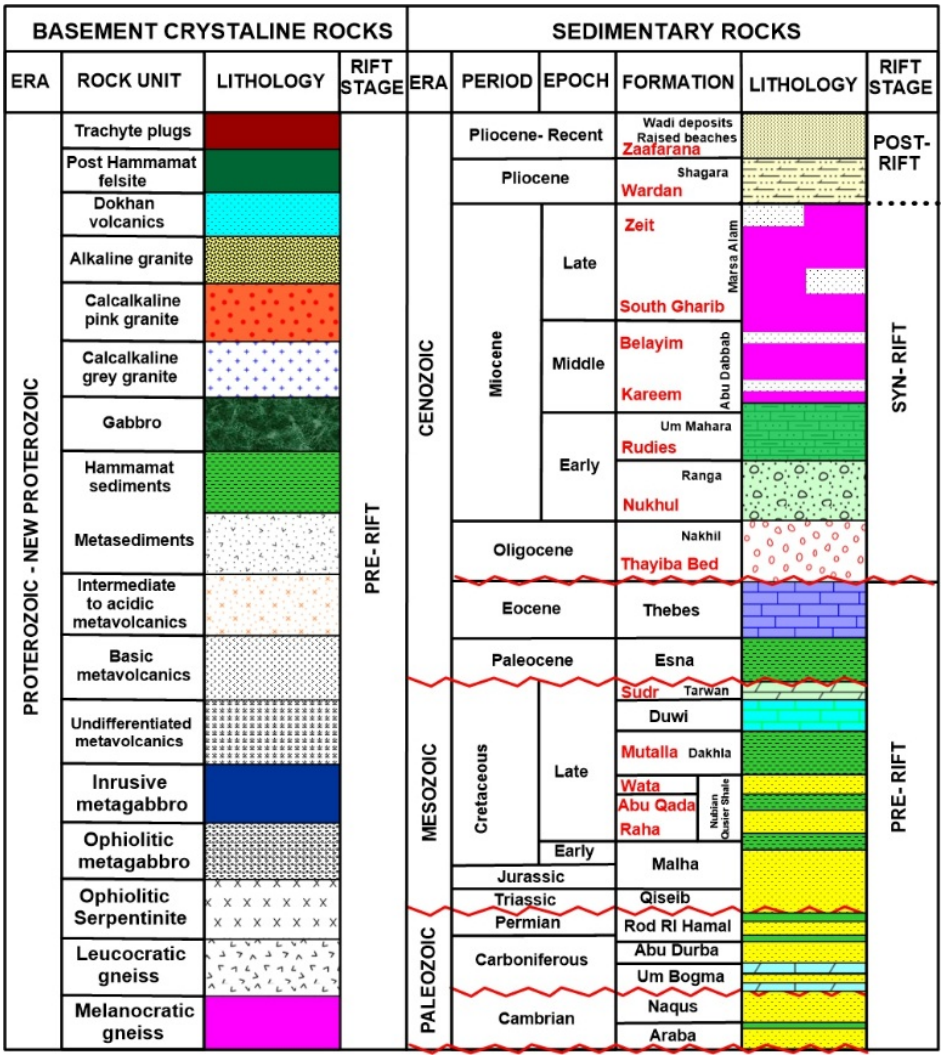

Figure 3. Stratigraphic column of the NRS and the Gulf of Suez. Modified after Amer et al., 2012. The red color shows the formation names that are used by petroleum companies.

3. DATA AND METHODOLOGY

3.1. Magnetic Data

This research is carried out depending mainly on the reduced to pole (RTP) aeromagnetic data (Fig. 4) with a contour interval of 20 nT, scale 1:250,000 (total field of the area is 41,400 nT, the inclination angle is 37.4 degrees and the declination angle is +1.6 degrees). These data were compiled for the NRS area by Censa 404 titans (N80DS) aircraft using Varian V-85 Proton Precession Magnetometer. The main parameters of this survey include (1) the altitude, which was 500 feet; (2) the station spacing was 1km traverse and 5km tie lines and (3) the flight line direction was traverse= 50° / 23° and tie line= 140°/ 320°. The survey was collected by Meshref (1990) and obtained from Saad (1991).

3.2. Determination of the Curie point depth (CPD)

Magnetic anomalies come from both the near-surface and the far-surface magnetic bodies (Thébault et al., 2010). Consequently, the magnetic data contain high wavenumbers and low wavenumbers anomalies together. The high wavenumbers anomalies, which are characterized by short-wavelengths, come from topography and/or near-surface magnetic sources. On the other hand, major low wavenumbers components, which are characterized by long-wavelengths, originate from regional features and the main magnetic core fields that possibly can affect the centroid depth estimations (Okubo et al., 1985; Tsokas et al., 1998; Stampolidis & Tsokas, 2002). The CPD assessment needs the deepest magnetic sources. The main magnetic core field had been removed by the application of the International Geomagnetic Reference Field (IGRF) to yield the RTP magnetic map (Fig. 4). The RTP map had been built to correct the position of the magnetic anomalies directly above their sources.

Spector & Grant (1970) adapted the basic 2-D spectral analysis technique to estimate the depth to the top of magnetized rectangular prisms (Zt) from the

slope of the logarithmic power spectrum. A Few years later, Bhattacharyya & Leu (1975 and 1977) computed the centroid depth (Z0) of the magnetic bodies. Okubo et al., (1985) proven this technique for assessing the bottom depth of the magnetic bodies (Zb).

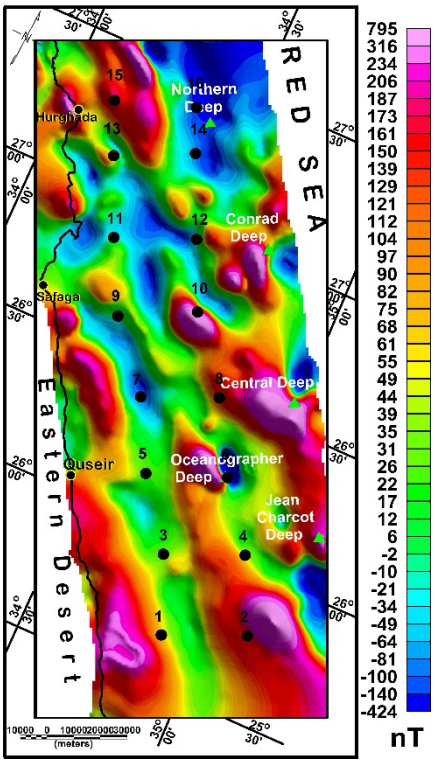

Figure 4. The reduced to pole (RTP) aeromagnetic map shows the deep brines and the sixteen blocks that were used to estimate the depth to the top (Z_t) and the centroid (Z_0) of the magnetic sources of the investigation area.

To define the Zt, a straight line should be fitted for the high-wavenumber part of the radially averaged power spectrum depending on the next procedure based on the method that was existed by Blakely (1995) and Tanaka et al., (1999):

$$\ln[\phi_{\Delta T}(|k|)^{1/2}] = \ln B - |k|Z_t \quad \ldots (1)$$

Where ($\phi_{\Delta T}$) is the entire magnetic field and (B) is a constant for the equation. Likewise, the Z0 of the magnetic centroid can be assessed by fitting a straight line overhead the low-wavenumber portion of the radially averaged frequency-scaled power spectrum as exposed in the next procedure:

$$\ln\{[\phi_{\Delta T}(|k|)^{1/2}]/|k|\} = \ln D - |k|Z_0$$

……(2)

Where (D) is the constant of the equation.

Therefore, Z_t and Z_0 of the magnetic layer can be determined. According to Okubo *et al*., 1985 and Tanaka et al., 1999, the basal depth (Z_b) of any magnetic source can be resulted as:

$Z_b = 2Z_0 - Z_t$…….. (3)

The acquired Z_b of the magnetic layer is identical to the CPD due to the increasing of temperature downward to the interior of the earth. At Z_b, Ferromagnetic minerals damage their magnetization at a temperature of approximately 580º C. Above this temperature, there is no magnetic polarization. Therefore, the depth of this temperature is the bottom of the magnetic layer. In fact, the Curie temperature of any rock depends mainly on its mineral composition. For example, the presence of Titanium in oceanic crust (Titanomagnetite) drops this temperature (about 350ºC). Because of the abundance of magnetite and its large magnetic contribution, nearly, all authors used its Curie temperature (580ºC) to determine the lower boundary of the crustal magnetic layer.

To connect Z_b with the Curie point isotherm (580ºC), a vertical path of temperature variation and a constant GG were supposed. The GG from the CPD (that identical to Z_b) up to the earth's surface can be resulted (Tanaka *et al*., 1999; Stampolidis et al., 2005, Maden 2010) by the next calculation:

$GG = 580ºC/Z_b$ ……. (4)

The Fourier's cooling law (Fourier, 1955) can be used to assess the HF values using the following calculation:

$Q = \lambda\ (580ºC/Z_b)$ …….... (5)

Where Q is the assessed HF and λ is the coefficient of the thermal conductivity. There are no conductivity measurements. Therefore, conductivities have to be assessed from the works (Girdler, 1970). For this study, the values of GG and HF are computed according to the Curie-temperatures of 580ºC and the thermal conductivity of 2.5 W/m°C that were computed by Stacey (1977) for igneous rocks (Figure 3) and used by different authors all over the world. In addition, it depends also on the lithology as explained in Morgan et al., (1983).

Bhattacharyya & Leu (1977) indicated that the shape of lonely magnetic anomalies could be used to estimate the CPD of the magnetic layer. In addition, Shuey et al., (1977) utilized the form of the magnetic anomalies to assess CPD. They showed that it was not possible to realize this thickness in space domain and so, used the frequency domain (spectral analysis method).

In different localities around the world, the magnetic data were used for assessing the CPD by applying the spectral analysis technique to these data. To apply this technique, the considered areas were divided into square blocks (Blakely (1988), Tanaka et al., (1999), Stampolidis & Tsokas (2002), Chiozzi et al., (2005), Trifonova et al. (2009), Aboud et al., (2011), Kasidi & Nur (2012), Hsieh et al., (2014), Abraham et al., (2014 and 2015), Selim & Aboud (2014), Gao et al., (2015) and Saada (2016b)).

According to Shuey et al,. (1977), the spectrum of any map has a maximum depth information not exceed to a depth of its length (L) divided by 2π. Therefore, the spectral analysis is utilized for computing the depth to the bottoms of magnetic forms that do not go above (L) /2π. If so, the spectral peak takes place at a frequency lower than the essential frequency for the map and cannot be resolved. However, Okubo *et al.* (1985) used the block sizes of dimension vary from 60 to 90km for their studies. Due to the restricted depth extent of the magnetized layer, magnetic anomalies at the earth's surface are damped at long wavelengths. Therefore, the dimensions of the used magnetic maps do not exceed 100 x 100km (Maus et al., 1997). Okubo et al., (1985) advised that centroid depth (Z_0) estimation could be derived from data windows as small as 40 x 40km. Generally, the rifting areas are characterized by their high HF and hence shallow CPD. Therefore, small windows can be used in high GG areas. On the road to calculate the CPD, the examination area was disjointed into sixteen overlapped square blocks with dimensions of 60 x 60km (Fig. 4). The squared zones are overlapped with 30km (50% of the squared areas). The middles of each block are used to plot the assessed CPD and HF. The CPD (Z_b) is realized by assessing the Z_t and Z_0 of magnetic causes as described in equation (3).

4. RESULTS

The positive and the negative magnetic anomalies with different sizes, forms, and extensions can be seen in the RTP magnetic map (Fig. 4). This variation suggests diverse in the depths, chemical/mineralogical compositions, and dimensions of the magnetic causes. The map also displays that most anomalies are aligned in the NNW to WNW directions with both sharp and gentle gradients. These trends explain that the investigation area was affected primarily by the RS extension system. The short wavelength anomalies with small extensions are concentrated in the northern and northeastern parts (east to Safaga and Hurghada cities). On the other hand, the southern part of Safaga city reveals both positive and negative anomalies with large extension and long wavelengths. The area shows a number of dipoles in the middle and eastern parts close to the rifting zone. In addition, linear anomalies with the NW directions at the southern parts reflect the monoclonal structures related to the RS rifting system.

The Z_t and Z_0 were resulted from the slopes of the second-longest wavelengths $\ln[\phi_{\Delta T}(|k|)^{1/2}]$ and the frequency-scaled power spectrum $\ln\{[\phi_{\Delta T}(|k|)^{1/2}]/|k|\}$, respectively. Therefore, the amplitude spectra of the high wavenumber portions were selected to fit Z_t via equation (1) but the low wavenumbers ones were carefully chosen to fit Z_0 via equation (2). In addition, the errors of fit for both Z_t and Z_0 were calculated using Grapher 9.1 software.

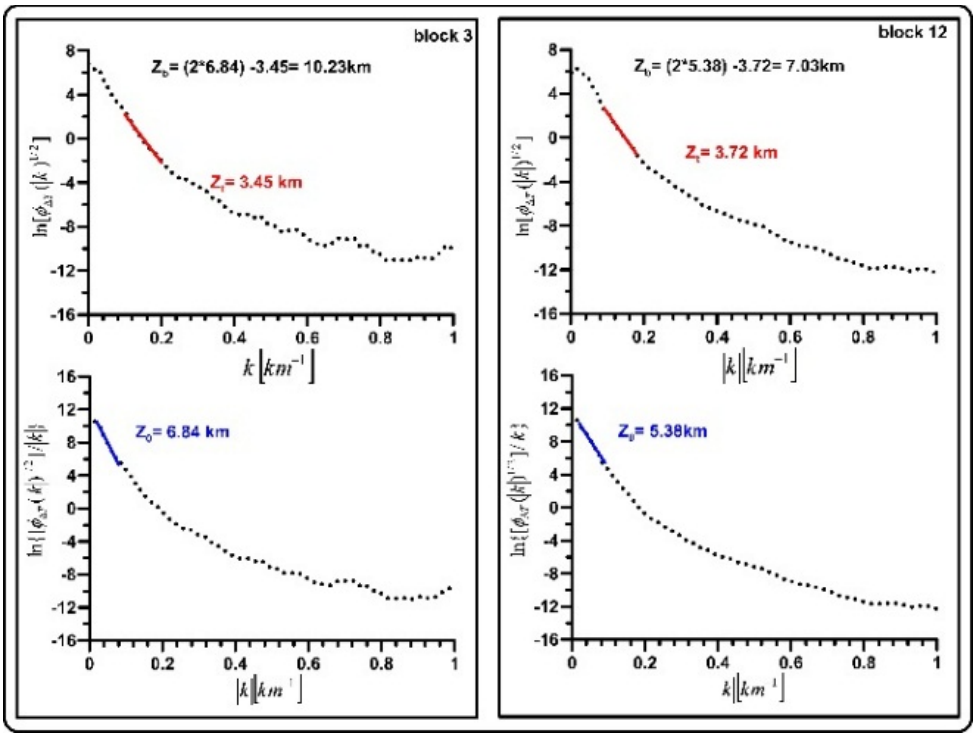

Figure 5. Examples of the radially average power spectrum for blocks 3 and 12.

Table 1. Results from applying spectral analysis and the mentioned equations to the divided blocks

Block No.	Z_t m)	Error Z_t	Z_0 km)	Error Z_0	Z_b (km)	d_T/d_Z (°C/km)	Q (mW/m^2)
1	4.1	0.01	9.51	0.10	14.9	37	92
2	3.4	0.01	8.24	0.07	13.1	42	105
3	3.4	0.06	6.84	0.07	10.2	54	134
4	3.5	0.08	6.53	0.15	9.5	58	145
5	4.4	0.07	6.92	0.13	9.4	58	146
6	4.2	0.05	6.82	0.06	9.5	58	145
7	4.0	0.03	5.82	0.19	7.6	72	180
8	5.5	0.13	6.45	0.16	7.4	74	185
9	3.7	0.07	6.11	0.20	8.5	64	161
10	3.9	0.13	6.10	0.13	8.3	67	166
11	4.3	0.05	5.95	0.17	7.6	72	180
12	3.7	0.01	5.38	0.08	7.0	78	196
13	3.2	0.13	7.05	0.09	10.9	50	126
14	4.5	0.00	5.92	0.12	7.4	74	186
15	3.6	0.21	7.23	0.19	10.8	51	127
16	4.1	0.01	6.66	0.14	9.2	60	150
Minimum	3.2	0	5.38	0.06	7	37	92
Maximum	5.5	0.21	9.51	0.2	14.9	78	196
Mean	3.97	0.07	6.72	0.13	9.5	60.6	151.5

Figure 5 displays two examples of the radial power spectrum design for blocks 3 and 12. The Z_b, d_T/d_Z and the surface HF, as well as their statistical readings are appraised and scheduled in Table 1. The assessed CPD varies from 7 to 14.9km. The GG ranges from 37 to 78°C/km and the HF from 92 to 196mW/m^2.

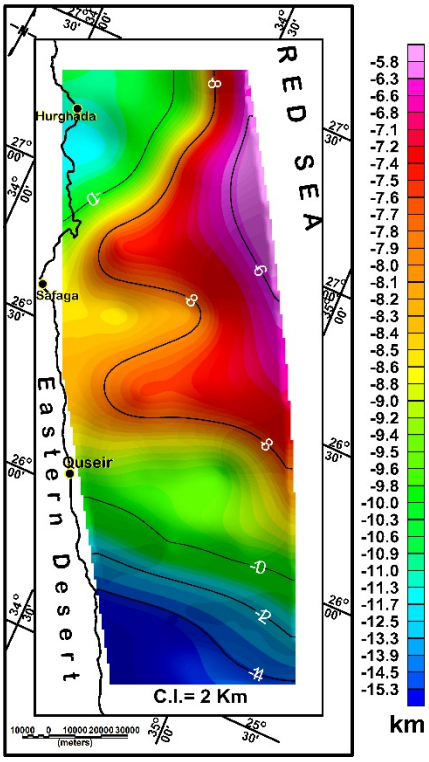

Figure 6. CPD map of the study area.

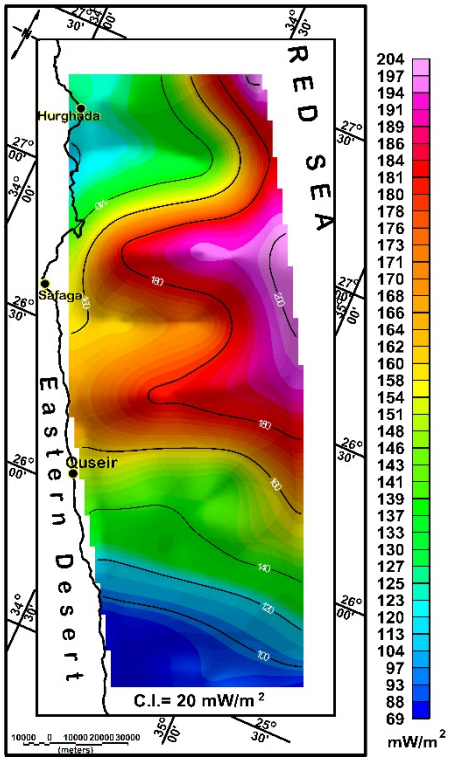

Figure 7. Heat flow (HF) map of the study area.

These results were plotted at the center of each block then contoured to construct the CPD map of the Egyptian NRS shelf (Fig. 6). It shows a noticeable decrease toward the axial trough. The greatest CPD lies in the southwestern corner (south to Quseir city) while the smallest values locate east to Safaga and

Hurghada cities. The estimated surface HF (Fig. 7) exposes a strong trend decreases from the offshore part toward the western onshore region.

5. DISCUSSION

To estimate the HF from magnetic data, the CPD that correspond to the bottom of magnetic sources must be determined. Previously, it was assumed that the lower magnetic boundary is controlled by the vertical change in the rock composition. As, Wasilewski et al., (1979) considered that the Moho discontinuity is the lower magnetic boundary due to the non-appearance of magnetite in the upper portion of the mantle. Lately, Friedman et al., (2012) examined the magnetization for some samples of the upper mantle. They found few quantities of magnetic minerals in the theses samples. This few quantities reveal a significant contribution to the magnetic properties of the examined samples. Accordingly, Friedman et al., (2012) deduced that the long-wavelength magnetic anomalies come from the effect of such few quantities in the upper mantle. In addition, Ferré et al., (2013) declared that the xenolith specimens of the upper mantle of the low geothermal regions keep up a giant magnetic remanence. Consequently, many authors connected the lower magnetic boundary with high temperatures at depth, which cause losing the magnetic polarization of the rocks i.e., beneath the CPD (Connard et al., 1983) whether this depth can be recorded above or below the Moho discontinuity.The spectral analysis was applied to these RTP data (using Oasis Montaj, 2007) to yield the depth of the basal magnetic layer, GG, and the HF as explained previously. The resulted HF map shows a general increase towards the rifting zone (Fig. 7).

Augustin et al., (2014) and Mitchell & Park (2014) likewise examined the progress to spreading of the RS. Rasul & Stewart (2015) explained that the continental crust of the RS margins undergoes a noticeable thinning due to the birth of a new ocean. Glassley (2010) indicated that the oceanic crust has little radioactive elements because it comes from the mantle. On the contrary, the continental crust has greater radioactive elements as compared with the oceanic one. Therefore, if this thinning is the main HF controlled factor, the HF should decrease toward the rift zone. The results of figures (6) and (7) reflect an obvious CPD decrease and HF increase in that direction. Consequently, the results of this study cannot be interpreted as a result of the crustal thinning of the African continental crust. The rifting zone is characterized by thin crust with magmatic convection currents beneath it. These currents come from the upper mantle, which moves the African and the Arabian plates away from each other to form the RS depression. They are associated also with the formation of normal faulting and the intrusion of magmatic bodies. These reasons control the HF within the study area and interpret the CPD decrease and the HF increase to the direction of the main trough (more than 196 mW/m^2).

Typically, the CPD is controlled by the amount of the upwelling HF. Within any region, the geothermal flow depends upon (1) the richness of the radioactive minerals contained by the crust, (2) the tectonic setting of that region, and (3) the degree of the uprising HF from the mantle underneath it (Stein, 1995). Therefore, in spite of the thinning of the continental crust that contains radioactive minerals, the tectonic setting of the NRS can be considered as the main reason of the great HF near the axial trough. As illustrated in Figure (4), the area has a number of the deeps, which are linked with obvious dipolar magnetic anomalies; indicating a presence of new, limited intrusions (Cochran et al., 1986). Martinez & Cochran (1988) interpreted these deeps, as the principal phases in the progress of a magmatic spreading axis within NRS. King & Metcalfe, 2013 established that rift zones could be considered as the greatest encouraged tectonic settings for unsighted geothermal systems. Rift zones occur where lithospheric plates (African-Arabian) are thinned by tectonic extension and convection at zones of upwelling hot material. Ebinger & Sleep (1998) declared that any rift has usual channels for hot material from mantle plumes to stream horizontally below the thin lithosphere. Consequently, the great values of the HF at the eastern part of the examination area can be linked to this magmatic spreading. Abdel-aal & Yagi (2017) published the seismicity map in the NRS since 1900 to 2013 (Fig. 8). The correlation between Figs (6, 7) and the seismicity map (Fig. 8) shows that the activities of earthquakes are focused on the eastern portion of the study area, which has a shallow CPD and high GG as well as HF values. This activity reflects the great effect of the rifting action as compared with the thinning of the continental crust of the African plate to the east, where many earthquakes with different magnitudes are represented as displayed in the figure.

This study displays the detailed results as compared with the regional studies that were carried out by Saleh et al., (2013) and Elbarbary et al., (2018). It covers the offshore part of the studied area (40x40km) that was carried out by Salem et al., (2000) and gives similar results. In addition, the results are in agreeable with the geothermal measurements that were measured by Girdler &

Evans (1977) and Martinez & Cochran (1989). This study can also be correlated with the results that were coming from magnetic data of the area lies to the south of the study area by Saada (2016a). The area shows shallower CPD than the southern portion. This interprets the concentration of earthquake activity in this area as comared by the southern one (Fig. 8). However, both results show a general increase of the HF toward the axial trough.

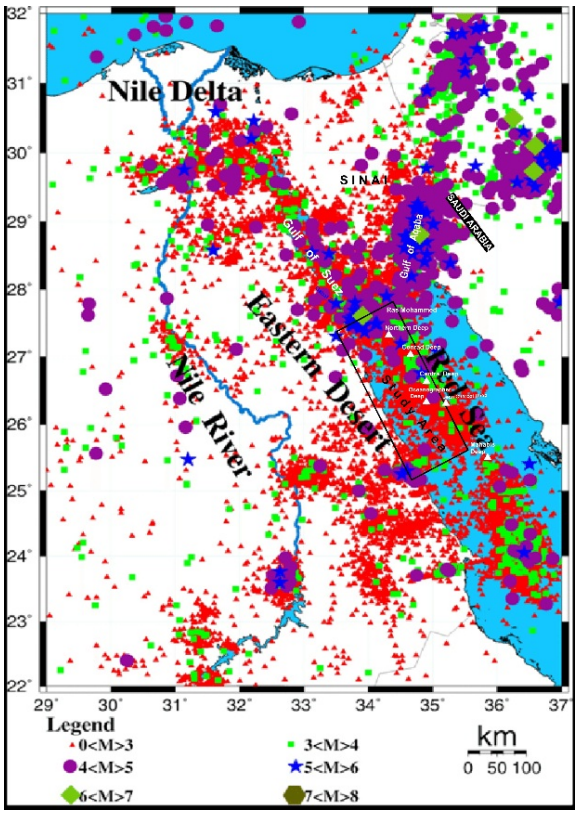

Figure 8. The instrumental seismicity in the NRS area (after Abdel-aal & Yagi, 2017).

6. CONCLUSION

The Spectral analysis had been applied to RTP aeromagnetic data to calculate the basal depth of the magnetized layer herein assumed CPD, beneath the Egyptian NRS region for assessing the HF. The magnetic data comprises the effects originated from both near-surface and deep magnetic sources. The estimation of CPD is related to these deeper sources.

CPD increases from 7km (close to the rifting axis) to about 15km at the southwestern part. This reflects a common GG decreasing of roughly 78 to 37˚C/km westward. In addition, the surface HF ranges from about 92 to 196 mW/m^2. Accordingly, the area reveals a high GG and HF regularly near to the rifting area. This high HF of the area as a part of the rifting system of the RS exhibits the important contribution of the uprising HF from the mantle below.

The importance of this study comes from the unexplored area of petroleum despite the availability of different geological structures and rocks in addition to the GG, which helps in the formation of oil and gas. The second point comes in terms of the need for renewable energy sources, where the NRS region is the most abundant areas of Egypt for the geothermal energy source. In Egypt, the Ministry of Electricity and Renewable Energy is planning to exploit the coastal strip of the RS to generate the geothermal energy with a width of 30 km extending from Ain Sukhna (in the GOS) and to the Southern part of Marsa Alam. In general, RS countries can use the geothermal energy in various ways ranging from heating purposes to generating electricity.

REFERENCES

Abdel-aal, A.K. & Yagi, Y., 2017. *Earthquake source characterization, moment tensor solutions, and stress field of small-moderate earthquakes occurred in the northern Red Sea Triple Junction.* Geosci J, 1-17 doi: 10.1007/s12303-016-0025-x.

Abdelsalam, M.G. & Stern, R.J., 1996. *Sutures and Shear Zones in the Arabian Nubian Shield.* J Afr earth sci, 23(3),289-310. doi:10.1016/S0899-5362(97)00003-1

Aboud, E., Salem, A. & Mekkawi, M., 2011. *Curie depth map for Sinai Peninsula, Egypt deduced from the analysis of magnetic data.* Tectonophysics 506, 46–54.

Abraham, E.M., Lawal, K.M., Ekwe, A.C., Alile, O., Murana, K.A. & Lawal, A.A., 2014. *Spectral analysis of aeromagnetic data for geothermal energy investigation of Ikogosi Warm Spring - Ekiti State, southwestern Nigeria.* Geotherm energy 2, 6.21p

Abraham, E.M., Obande, E.G., Chukwu, M., Chukwu, C.G. & Onwe, M.R., 2015. *Estimating depth to the bottom of magnetic sources at Wikki Warm Spring region, northeastern Nigeria, using fractal distribution of sources approach.* Turk J Earth Sci, 24 doi: 10.3906/yer-1407-12.

Allan, T.D., 1970. *Magnetic and gravity fields over the Red Sea.* Philos. Trans. R. Soc. London, A267, 153-180.

Amer, R., Sultan, M., Ripperdan, R. & Encarnación, J., 2012. *Structural Architecture for Development of Marginal Extensional Sub-Basins in the Red Sea Active Rift Zone*. IJG, 3, 133-152.

Augustin, N., Devey, C.W., Van der Zwan, F.M., Feldens, P., Tominaga, M., Bantan, R.A. & Kwasnitschka, T., 2014. *The rifting to spreading transition in the Red Sea.* Earth Planet Sci Lett 395, 217-230.

Avigad, D. & Gvirtzman, Z., 2009. *Late Neoproterozoic Rise and Fall of the Northern Arabian-Nubian Shield: The Role of Lithospheric Mantle Delamination and Subsequent Thermal Subsidence.* Tectonophysics, 477(3-4), 217-228. doi:10.1016/j.tecto.2009.04.018.

Backer, B.H. & Schoell, M., 1972. *New deeps with brines and metalliferous sediments in the Red Sea*. Nature (London), Phys ScL 240, 153-158.

Becker, J.J., Sandwell, D.T., Smith, W.H.F., Braud, J., Binder, B., Depner, J., Fabre, D., Factor, J., Ingalls, S., Kim, S.H., Ladner, R., Marks, K., Nelson, S., Pharaoh, A., R. Trimmer , Von Rosenberg, J., Wallace, G. & Weatherall, P., 2009.*'Global Bathymetry and Elevation Data at 30 Arc Seconds Resolution: SRTM30_PLUS,* Mar Geod, 32 (4), 355 – 371.

Bertram, C., Krätschell, A.O.,'Brien, K., Brückmann, W., Proelss, A. & Rehdanz, K., 2011. *Metalliferous sediments in the Atlantis II Deep-assessing the geological and economic resource potential and legal constraints.* Resour Policy, 36, 315-329.

Bhattacharyya, B.K. & Leu, L.K., 1975. *Analysis of magnetic anomalies over Yellowstone National Park. Mapping the Curie-point isotherm surface for geothermal reconnaissance.* JGR, 80, 461-465.

Bhattacharyya B.K. & Leu, L.K., 1977. *Spectral analysis of gravity and magnetic anomalies due to rectangular prismatic bodies.* Geophysics, 42, 41-50.

Blakely, R.J., 1995. *Potential theory in gravity and magnetic applications.* Cambridge University Press, 307-308.

Blakely, R.J., 1988. *Curie temperature isotherm analysis and tectonic implications of aeromagnetic data from Nevada*, JGR, 93 (11), 817 - 832.

Bosworth, W., Huchon, P. & McClay, K., 2005. *The Red Sea and Gulf of Aden Basins.* J Afr Earth Sci, 43(1-3), 334-378. doi:10.1016/j.jafrearsci.2005.07.020

Botz, R., Schmidt, M., Kus, J., Ostertag-Henning, C., Ehrhardt, A., Olgun, N., Garbe-Schonberg, D. & Scholten, J., 2011. *Carbonate recrystallization and organic matter maturation in heat-affected sediments from the Shaban Deep, Red Sea.* Chem Geol 2801-2), 126-143.

Boulos, F.K., *Some aspects of the geophysical regime of Egypt in relation to heat flow, groundwater and microearthquakes,* in R. Said (ed.), The Geology of Egypt, A.A. Balkema Rotterdam 1990, pp. 61-89.

Byerly, P.E. & Stolt, R.H., 1977. *An attempt to define the Curie point isotherm in northern and central Arizona.*Geophysics 42, 1394-1400.

Chiozzi, P., Matsushima, J., Okubo, Y., Pasquale, V. & Verdoya, M., 2005. *Curie-point depth from spectral analysis of magnetic data in central–southern Europe.* PEPI,152, 267-276..

Cochran, J.R., 2005. *Northern Red Sea: nucleation of an oceanic spreading center within a continental rift.* G3, doi:10.01029/02004GC000826

Cochran, J.R. & Martinez,, F., 1988. *Evidence from the northern Red Sea on the transition from continental to oceanic rifting:* Tectonophysics 153, 25-53.

Cochran, J.R., Rtinez, F., Steckler, M.S. & Hobart, M.A., 1986. *Conrad Deep a new northern Red Sea deep: Origin and implications for continental rifting*: Earth Planet Sci Lett 78 (1), 18-32.

Connard, G., Couch, R. & Gemperle, M., 1983. *Analysis of Aeromagnetic measurements from the Cascade Range in central Oregon.* Geophysics, 48, 376-390.

Cousteau, J.Y., Nesteroff, W. & Tazieff, H., 1953. *Coupes transversales de la Mer Rouge, Comptus Rendus Congres* Geologique International, 19th Session Sect. IV.

Ebinger, C. & Sleep, N.H., 1998. *Cenozoic magmatism in central and east Africa resulting from impact of one large plume*. Nature, 395, 788–791.

Egloff, F., Rihm, R., Makris, J., Izzeldin, Y.A., Bobsien, M., Meier, K., Junge, P., Noman, T. & Warsi, W., 1991. *Contrasting structural styles of the eastern and western margins of the southern Red Sea: the 1988 SONNE experiment.* Tectonophysics 198, 329-353.

Ehrhardt, A. & Hübscher, C., 2003. *Preliminary results-geophysics. Meteor Berichte.* In: Pätzold J, Bohrmann G, Hübscher C (eds), Meteor Berichte M52 Black Sea, Mediterranean-RS 3, 3-21.

Elbarbary, S., Abdel Zaher, M., Mesbah, H., El-Shahat, A. & Embaby A., 2018. *Curie point depth, heat flow and geothermal gradient maps of Egypt deduced from aeromagnetic data*. Renewable and Sustainable Energy Reviews, 91, 620–629.

Feinstein, S., Kohn, B.P., Steckler, M.S. & Eyal, M., 1996. *Thermal history of the eastern margin of the Gulf of Suez* .1. Reconstruction from borehole temperature and organic maturity measurements. Tectonophysics 266, 203-220.

Ferré, E.C., Friedman, S.A., Martín-Hernández, F.A., Feinberg, J.M., Conder, J.A. & Ionov, D.A., 2013. *The magnetism of mantle xenoliths and potential implications for sub-Moho magnetic sources.* Geophys Res Lett, 40, 105-110 doi: 10.1029/2012GL054100

Fourier, J., 1955. Analytical Theory of Heat. Dover Publications New York.

Friedman, S.A., Ferré, E.C., Martín-Hernández, F.A., Feinberg, J.M., Ionov, D.A. & Conder, J.A., 2012. *What is Magnetic in the mantle? Insights into magnetic minerals in mantle xenoliths.* EGU General Assembly, 2012 held 22-27 April, Vienna, Austria, 13747 p

Gao, G., Kang, G., Bai, C. & Wen, L., 2015. *Study on crustal magnetic anomalies and Curie surface in Southeast Tibet.* J Asian Earth Sci, 97, 169–177.

Garfunkel, Z., 1981. *Internal Structure of the Dead Sea Leaky Transform (Rift) in Relation to Plate Kinematics.* Tectonophysics, 80(1-4), 81-108. doi:10.1016/0040-1951(81)90143-8.

Garfunkel, Z. & Ben-Avraham, Z., 1996. *The Structure of the Dead Sea Basin.* Tectonophysics, 266(1-4), 155-176.doi:10.1016/S0040-1951(96)00188-6.

Gaulier, J.M., Le Pichon, X., Lyperis, N., Avedlik, F., Geli, L., Moretti, I., Deschamps, A. & Salah, H., 1988. *Seismic study of the crust of the northern Red Sea and Gulf of Suez.* Tectonophysics 153, 55-88.

Ghebreab, W., 1998. *Tectonics of the Red Sea Region Reassessed.* Earth Sci Rev, 45(1-2), 1-44. doi:10.1016/S0012-8252(98)00036-1.

Girdler, R.W., 1970. *A review of Red Sea heat flow.* Phil

Trans Roy Soc Lond, 267(1181), 191-203.

Girdler, R.W. & Evans, T.R., 1977. *Red sea heat flow.* Geophys J R Astr Soc, 51, 245- 251.

Glassley, W.E., 2010. *Geothermal Energy: Renewable Energy and the Environment.* CRC Press Taylor & Francis Group USA, 276 p.

Hartmann, M., 1980. *Atlantis II Deep geothermal brine system. Hydrographic situation in 1977 and changes since 1965*. Deep Sea Res. Part A Oceanogr Res Pap 27 (2), 161-164, IN3-IN4, 165-171.

Hosney, H., 2001. *An introduction to the geothermal regime and its tectonic implications of the Suez Rift System.* JOES, 22, 157-182.

Hosney, H.M., 2000. *Geophysical parameters and crustal temperatures characterizing tectonic and heat flow provinces of Egypt.* Cairo Uni., Egypt Sep, 152- 166.

Hsieh, H.H., Chieh, H.Ch., Pei, Y. & Horng, Y.Y., 2014. *Curie point depth from spectral analysis of magnetic data in Taiwan.* Journal of Asian Earth Sciences 90, 26-33.

Issawi, B., Francis, M., El Hinnawy, M., Mehanna, A. & El Deftar, T., 1971. *Geology of the Safaga-Quseir Coastal Plain and of Mohamed Rabah Area.* Ann Geol Surv Egypt, 1, 1-19.

Kasidi, S., Nur, A., 2012. *Curie depth isotherm deduced from spectral analysis of Magnetic data over sarti and environs of North-Eastern Nigeria.* ISRN Biotechnology, 1(3), 49-56.

King, D. & Metcalfe, E., 2013. *Rift zones as a case study for advancing geothermal occurrence models. In: 38th Workshop on Geothermal Reservoir Engineering*, Stanford Uni, Stanford, California, 11.

Laughton, A.S., 1970. *A new bathymetric chart of the Red Sea.* Royal Soc. London Philos Trans. Ser A 267, 21-22.

Ligi, M., Bonatti, E., Tontini, C.F., Cipriani, A., Cocchi, L., Schettino, A., Bortoluzzi, G., Ferrante, V., Khalil, S.M., Mitchell, N.C. & Rasul, N., 2011. *Initial Burst of Oceanic Crust accretion in the Red Sea due to edge-driven mantle convection.* Geology, 39, 1019-1022. doi:10.1130/G32243.1

Maden, N., 2010. *Curie-point depth from spectral analysis of magnetic data in Erciyes stratovolcano (Central TURKEY).* Pure Appl Geophys, 167, 349-358.

Maden, N., 2012. *Two-dimensional geothermal modeling along the Central Pontides magmatic arc (Northern Turkey).* Surv Geophys, 33, 275-292.

Maden, N., Gelisli, K., Eyuboglu, Y. & Bektas, O., 2009. *Determination of tectonic and crustal structure of the Eastern Pontide Orogenic Belt (NE Turkey).* Pure Appl Geophys, 166, 1987-2006.

Makris, J. & Rihm, R., 1991. *Shear-controlled evolution of the Red Sea: pull apart model.* Makris J, Mohr P, Rihm R (Eds). Tectonophysics 198, 441-466.

Martinez, F. & Cochran, J.R., 1988. *Structure and tectonics of the northern Red Sea: catching a continental margin between rifting and drifting.* Tectonophysics 150, 1-32.

Martínez, F. & Cochran, J.R., 1989. *Geothermal measurements in the northern Red Sea: implications for lithospheric thermal structure and mode of extension during continental rifting.* J Geophys Res, 94 (12), 239-12,265.

Maus, S., Gordon, D. & Fairhead, D., 1997. *Curie temperature depth estimation using a selfsimilar magnetization model.* JGR, 129, 163-168.

Meshref, W.M., 1990. *Tectonic framework.* In: Said R (Ed.). The Geology of Egypt. A.A. Balkema Rotterdam, 113-155.

Miller, M. & Dixon, T., 1992. *Proterozoic Evolution of the Northern Part of the Hamisana Zone, Northeast Sudan: Constraints on Pan-African Accretionary Tectonics*, J Geol Soc London, 149, 743-750.

Mitchell, N.C. & Park, Y., 2014. *Nature of crust in the central Red Sea and topographic control of evaporite flowage.* Tectonophysics, 628, 123-139. doi:10.1016/j.tecto.2014.04.029.

Montenat, C., D'estevou, P., Purser, B., Burollet, P., Jarrige, J., Sperber, F., Philobbos, E., Plaziat, J., Prat, P., Richert, J., Roussel, N. & Thiriet, J., 1988. *Tectonic and Sedimentary Evolution of the Gulf of Suez and the Northwestern Red Sea.* Tectophysics, 153(1-4), 161-177. doi:10.1016/0040-1951(88)90013-3.

Moores, E.M., Twiss, R.J., *Tectonics.* Freeman, W.H. and Company, New York, 1995, 415p

Morgan, P., Boulos, F.K., Hennin, S.F., EI-Sherif, A.A., El-Sayed, A.A., Basta, N.Z. & Melek, Y.S., 1985. *Heat flow in Eastern Egypt: The thermal signature of a continental breakup*. J Geody 4, 107-131.

Morgan, P., Boulos, F.K. & Swanberg, G.A., 1983. *Regional geothermal Exploration in Egypt.* Geophys Pr, 31, 361-376.

Morgan, P. & Swanberg, C.A., 1979. *Heat flow and the geothermal potential of Egypt.* Birkhauser Verlag, Basel Pageoph, 117, 213-225.

Morgan, P., Swanberg, C.A., Boulos, F.K., Hennin, S.F., El-Sayed, A.A. & Basta, N.Z., 1980. *Geothermal studies in northeast Africa*, Ann Geol Surv Egypt 10, 971-987.

Oasis Montaj, 2007. *Geosoft Mapping and Application System*, Inc, Suit 500, Richmond St. West Toronto, ON Canada N5SIV6.

Okubo, Y., Graf, R.J., Hansent, R.O., Ogawa, K. & Tsu, H., 1985. *Curie point depths of the island of Kyushu and surrounding areas Japan*. Geophysics 53, 481-494.

Rasul, N.M.A. & Stewart, I.C.F., 2015. *The Red Sea: the formation, morphology, oceanography and environment of a young ocean basin.* Springer, 638 p.

Ries, A.C., Shackleton, R.M., Graham, R.H. & Fitches, W.R., 1983. *Pan-African Structures, Ophiolites and Mélange in the Eastem Desert of Egypt: A Traverse at 26˚N.* J Geol Soc London, 140(1), 75-95. doi:10.1144/gsjgs.140.1.0075.

Roeser, H.A. 1975. *A detailed magnetic survey of the southern Red Sea*. Geol Jahr, 13, 131-153.

Saad, M.H., 1991. *Geophysical study of Red Sea area, from Ras Mohamed to Ras Benas*, PhD thesis, Cairo Uni,

224p.

Saada, S.A., 2016a. *Geothermal reconnaissance of the area between Marsa Alam and Ras Banas, northern Red Sea*, Egypt, using aeromagnetic data. J Afr Earth Sci, 118, 45- 52.

Saada, S.A., 2016b. *Curie point depth and heat flow from spectral analysis of aeromagnetic data over the northern part of Western Desert, Egypt.* J Appl Geophy, 134, 100–111.

Said, R., 1962. *The geology of Egypt.* Amsterdam: Elsevier Scientific Publishing Co.

Said, R., 1990. The *Geology of Egypt.* Balkema Publishers, Rotterdam.

Saleh, S., Salk, M. & Pamukcu, O., 2013. *Estimating Curie Point Depth and Heat Flow Map for Northern Red Sea Rift of Egypt and Its Surroundings, from Aeromagnetic Data.* Pure Appl Geophys, 170, 863-885.

Salem, A., Ushijima, K., Elsirafi, A. & Mizunaga, H., 2000. *Spectral analysis of aeromagnetic data for geothermal reconnaissance of Quseir area, northern Red Sea, Egypt.* Proceedings World Geothermal Congress, Kyushu - Tohoku, Japan, 1669-1674.

Schmidt, M., Devey, C. & Eisenhauer, A., 2011. *FS Poseidon Fahrtbericht/Cruise Report P408-The Jeddah Transect; Jeddah-Jeddah, Saudi Arabia* 13.01.-02.03.2011 IFM-GEOMAR Report 46.

Scholten, J.C., Stoffers, P., Walter, P. & Plüger, W., 1991. *Evidence for episodic hydrothermal activity in the Red Sea from the composition and formation of hydrothermal sediments, Thetis Deep.* Tectonophysics, 190 (1), 109-117.

Selim, E.I. & Aboud, E., 2014. *Application of spectral analysis technique on ground magnetic data to calculate the Curie depth point of the eastern shore of the Gulf of Suez, Egypt.* Arab J Geosci, 7, 1749-1762.

Shuey, R.T., Schellinger, D.K., Tripp, A.C. & Alley, L.B., 1977. *Curie depth determination from aeromagnetic spectra.* Geophys J R Astron Soc, 50, 75-101

Smith, R.B., Shuey, R.T., Fridline, R.O., Otis, R.M. & Alley, L.B. 1974. *Yellowstone hot spot. New magnetic and seismic evidence.* Geology 2, 451-455.

Smith, W.H.F. & Sandwell, D.T., 1997. *Global sea floor topography from satellite altimetry and ship depth soundings.* Sci Mag, 277, 1956- 1962.

Spector& A., Grant, F.S., 1970. *Statistical models for interpreting aeromagnetic data.* Geophysics 35, 293-302.

Stacey, F.D., 1977. *Physics of the Earth:* NewYork, John Wiley and Sons, 2nd ed., 414p

Stampolidis, A., Kane, I., Tsokas, G.N. & Tsourlos, P., 2005. *Curie point depths of lbania inferred from ground total field magnetic data.* Surv Geophys, 26, 461-480.

Stampolidis, A. & Tsokas, G.N., 2002. *Curie point depths of Macedonia and Thrace, N Greece,* Pure Appl Geophys, 159, 2659-2671.

Stein, C.A., 1995. *Heat Flow of the Earth.* Amwrican Geophysical Union, Global Earth Physics, a Handbook of Physical Constants, 144-158.

Stern, R.J. & Hedge, C.E. 1985. *Geochronologic and Isotopic Constraints on Late Precambrian Crustal Evolution in the Eastern Desert of Egypt,* American Journal of Science, 285, 97-l27.

Stern, R.J., Johnson, P., Kröner, A. & Yibas, B., 2004. *Neoproterozoic Ophiolites of the Arabian-Nubian Shield.* In: Kusky, T. M. Ed., Precambrian Ophiolites and Related Rocks. Elsevier, Amsterdam, 95-128. doi:10.1016/S0166-2635(04)13003-X.

Sultan, M., Arvidson, R.E., Duncan, I.J., Stern, R.J. & Elkaliouby, B., 1988. *Extension of the Najd Shear System from Saudi-Arabia to the Central Eastern Desert of Egypt Based on Integrated Field and Landsat Observations.* Tectonics, 7(6), 1291-1306. doi:10.1029/TC007i006p01291.

Tanaka, A., Okubo, Y. & Matsubayashi, O., 1999. *Curie point depth based on spectrum analysis of the magnetic anomaly data in East and Southeast Asia,* Tectonophysics 306, 461-470.

Tazieff, H., 1952. *Une recente campagne oceanographique dans la mer Rouge,* Bull Soc Beige de Geol 61, 84-90.

Thébault, E., Purucker, M., Kathryn, A., Langlais, W.B. & Sabaka, T.J., 2010. *The magnetic field of the earth's lithosphere.* Space Sci Rev, 155, 95-127.

Trifonova, P., Zhelev, Zh., Petrova, T. & Bojadgieva, K., 2009. *Curie point depths of Bulgarian territory inferred from geomagnetic observations and its correlation with regional thermal structure and seismicity.* Tectonophysics, 473, 362-374.

Tsokas, G.N., Hansen, R.O. & Fytikas, M., 1998. *Curie point depth of the island of Crete (Greece),* Pure Appl Geophys, 152, 747-757.

Vine, F.J., 1966. *Spreading of the ocean floor-new evidence.* Science, 154, 1405-1415.

Wasilewski, P.J., Thomas, H.H. & Mayhew, M.A., 1979. *The Moho as a magnetic boundary:* Geophys Res Lett, 6, 541-544.

Winckler, G., Kipfer, R., Aeschbach-Hertig, W., Botz, R., Schmidt, M., Schuler, S. & Bayer, R., 2000. *Sub sea floor boiling of Red Sea Brines- new indication from noble gas data.* Geochimica et Cosmochimica Acta, 64(9), 1567-1575, doi.org/10.1016/S0016-7037(99)00441-X.

Yeats, R.S., Sieh, K. & Allen, C.R., 1997. *The Geology of Earthquakes.* Oxford University Press, Oxford.

Received at: 15. 12. 2018
Revised at: 29. 03. 2019
Accepted for publication at: 30. 03. 2019
Published online at: 02. 04. 2019